

PAPER

[View Article Online](#)
[View Journal](#)

Cite this: DOI: 10.1039/d5im00028a

Continuous direct air capture and conversion tandem system applicable to a wide range of CO₂ concentrations†Shinta Miyazaki, ^a Akihiko Anzai, ^{*a} Masaki Yoshihara,^a Hsu Sheng Feng,^a Shinya Mine, ^b Takashi Toyao ^a and Ken-ichi Shimizu ^{*a}

The concentrations of CO₂ emitted from different CO₂ sources vary significantly. Thus, processes capable of accommodating a broad range of CO₂ concentrations, from 0.04% (air) to 10% (power plants), must be developed to achieve carbon neutrality. In this study, we developed a two-step CO₂ capture and hydrogenation system by employing Rb-oxide-incorporated zeolites as CO₂ adsorbents and Ni/CeO₂ or Cu/ZnO/Al₂O₃ as catalysts for CO₂ hydrogenation. This process is suitable for continuous operation over a temperature swing of 40–200 °C. Notably, this system can operate at low temperatures (below 200 °C) using a simple temperature-swing process in the presence of O₂. Compared with more than 100 previously reported systems that can convert CO₂ including O₂ to green fuels such as CO or CH₄, the proposed system achieved the best CO₂ conversions to CH₄ and CO.

Keywords: Direct air capture (DAC); Zeolite sorbent; Temperature swing adsorption (TSA); Methanation; Reverse water-gas shift (RWGS).

Received 21st February 2025,
Accepted 12th June 2025

DOI: 10.1039/d5im00028a

rsc.li/icm

1 Introduction

Anthropogenic greenhouse gas emissions are critical in causing global warming.^{1,2} To mitigate global warming and achieve a carbon-neutral society, the amount of CO₂ emitted from energy- and industry-related sources must be significantly reduced.^{3,4} One of the most promising strategies for mitigating anthropogenic CO₂ emissions is to convert CO₂ into chemical fuels, such as methane or methanol, and value-added chemicals *via* syngas using green H₂ produced *via* water electrolysis using renewable energy sources such as wind and solar power.^{5,6} Large-scale production of green H₂ using water electrolysis has already been initiated at sites such as the Shell Energy and Chemicals Park Rheinland in Germany.⁷ These efforts highlight the increasing demand for practical CO₂ capture and utilization (CCU) technologies utilizing green H₂. However, in CCU technologies, CO₂ needs to be captured from emission sources (such as power, refinery, chemical, steel, and ceramic plants) and stored prior to chemical transformation.⁸ Although liquid amine

scrubbing is a commonly employed CO₂ capture and storage (CCS) technology in industry,⁹ it is hindered by high costs, significant energy requirements for solvent regeneration, and the need for large-scale plants.¹⁰

CO₂ needs to be captured from emission sources (such as power, refinery, chemical, steel, and ceramic plants) and stored prior to chemical transformation.⁸ Although liquid amine scrubbing is a commonly employed CO₂ capture and storage (CCS) technology in the industry,⁹ it is hindered by high costs, significant energy requirements for solvent regeneration, and the need for large-scale plants.¹⁰

Recently, unsteady-state CO₂ hydrogenation processes, known as CO₂ capture and reduction (CCR) and integrated CO₂ capture and conversion, have emerged as alternative technologies in which the need for CCS is avoided.^{11,12} In 2016, Urakawa *et al.*¹³ and Farrauto *et al.*¹⁴ separately published their works on CCR. Unlike conventional methods, CCR does not require large amounts of thermal energy for CO₂ separation and purification.¹⁵ Furthermore, this process is theoretically applicable to the utilization of O₂-containing CO₂ emitted from industries such as power plants and is advantageous for practical use.¹⁶

Dual-functional materials (DFMs) in which alkali or alkaline earth metals for CO₂ capture are combined with transition metals for CO₂ hydrogenation are widely used in CCR operations. Selective CH₄ and CO formation has been reported in various CCR studies (Table S1†). However, the

^a Institute for Catalysis, Hokkaido University, Sapporo, Hokkaido, Japan.E-mail: anzai.akihiro@cat.hokudai.ac.jp, kshimizu@cat.hokudai.ac.jp^b Research Institute for Chemical Process Technology, National Institute of Advanced Industrial Science and Technology, 4-2-1, Nigatake, Sendai, Miyagino-ku, Miyagi, Japan† Electronic supplementary information (ESI) available. See DOI: <https://doi.org/10.1039/d5im00028a>

reported CCR processes cannot be integrated with effluent streams released from various industrial processes because these are performed by changing the gas conditions stepwise (Fig. 1a). To address this, Urakawa *et al.* proposed a two-reactor parallel-type system for continuous CCR,¹³ whereas we developed a two-reactor parallel-type system for the continuous production of green fuels, such as CH₄^{17,18} and CO,^{19,20} from a CO₂ + O₂/N₂ mixture by alternating the feeds of CO₂ + O₂/N₂ and H₂ to the DFMs in the two reactors (Fig. 1b).

Our system can continuously capture low-concentration CO₂ (below 1%) from a mixture of O₂ and convert it into green fuels. However, continuous CCR is not applicable to high-concentration CO₂ emissions that are similar to exhaust gas emissions from thermal power plants and other industrial sources because of the limited CO₂ capacity of DFMs²¹ compared with zeolite sorbents.^{22,23} For example, less than 30% high-concentration inlet CO₂ (10%) can be converted even when one of the highest-activity DFMs available is used under optimized conditions (Fig. S1 and ESI† Text S1). This is because materials such as CaO—one of the most effective basic metal oxides used in DFMs—store CO₂ *via* a bulk diffusion mechanism, in which CO₂ must pass through CaCO₃ crystals to reach the unreacted CaO core.²⁴ Only surface carbonates are consumed during the reaction, while bulk carbonates remain inaccessible.²⁵ Consequently, this limitation restricts their applicability to dilute CO₂ streams. To effectively convert both diluted and high-concentration CO₂ (such as from thermal power plants and other industrial sources), it becomes essential to employ materials offering a range of adsorption site strengths and affinities. In contrast to DFMs, CO₂ can also be physically adsorbed onto sorbents like zeolites, enabling CO₂ adsorption and desorption under mild temperature swing conditions.^{26,27} However, removing the thermodynamic equilibrium constraint imposed by low temperatures to ensure high CO₂ conversion appears to be an insurmountable dilemma in continuous CCR. Accordingly, our central motivation was to overcome the limitation of CCR and

expand the application to a wide range of CO₂ concentrations, from direct air capture (DAC) to flue gas, while maintaining high performance.

In this study, we developed a novel system in which tandem CO₂ capture and hydrogenation are achieved by combining Rb-loaded zeolites (Rb-zeolites) as CO₂ adsorbents with CO₂ hydrogenation catalysts (Fig. 1c, and a detailed explanation of these three unsteady-state CO₂ hydrogenation processes is provided in ESI† Text S2). For CO₂ capture, zeolites were used as typical economically viable solid adsorbents. Unlike liquid and solid amines, zeolites do not produce toxic degradation products.²⁸ In addition, zeolites show greater stability than metal–organic frameworks (MOFs), which are also well-known solid adsorbents.^{29,30} For CO₂ hydrogenation, Ni/CeO₂^{31–33} and Cu/ZnO/Al₂O₃^{34–36} were used as typical catalysts for methanation and reverse water-gas shift (RWGS) reactions, respectively. Ni/CeO₂^{37–40} and Cu/ZnO/Al₂O₃,^{41–44} easily prepared by a simple method, are promising catalysts for the tandem system toward practical implementation. The sorbents were filled upstream in two parallel reactors. The catalyst was filled downstream in a single reactor. The system was based on continuous temperature swing adsorption (TSA) and catalytic reactions. Initially, a CO₂ + O₂/N₂ mixture was fed into the Rb-zeolite sorbent (denoted as Z) to capture CO₂ (eqn (1)). After this mixture changed to pure H₂ gas and the sorbent temperature was increased, the captured CO₂ and H₂ were simultaneously desorbed by applying heat (eqn (2)). Desorbed CO₂ and H₂ flowed to the bottom reactor, and the methanation or RWGS reaction proceeded using the catalysts (eqn (3) and (4)).

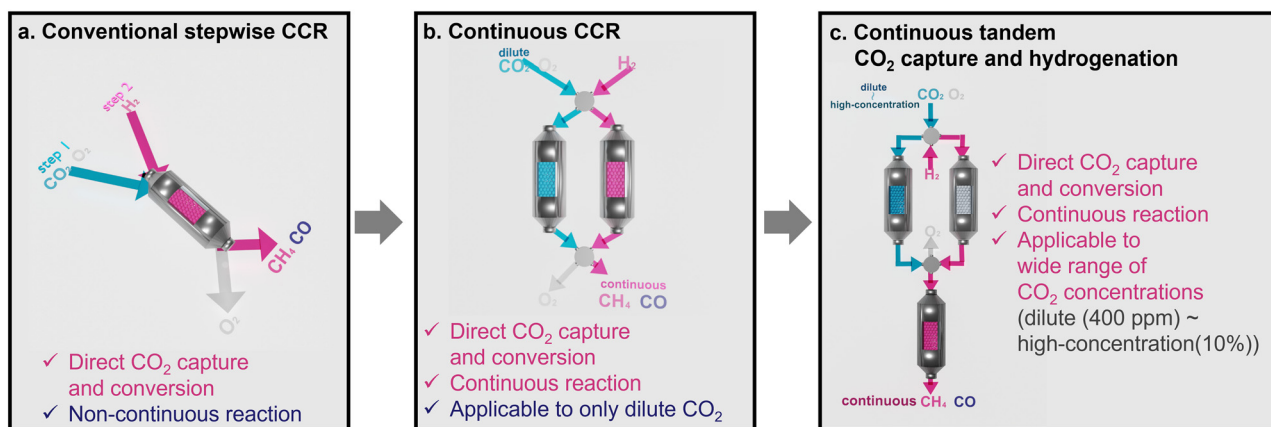
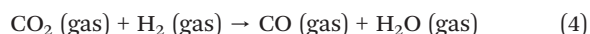
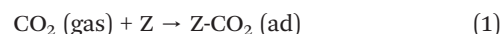


Fig. 1 Conceptual diagram of (a) conventional stepwise CCR, (b) continuous CCR, and (c) continuous tandem CO₂ capture and hydrogenation processes.



This new process is suitable for continuous operation under temperature-swing cycling in the low-temperature range (between 40 and 200 °C) in the presence of O₂. Compared with more than 100 reported CCR processes, this novel process exhibited high inlet CO₂ conversion.

2 Results and discussion

2.1 Screening and optimizing sorbents and catalysts

First, we examined the CO₂ adsorption properties of zeolite sorbents at 50 °C using a fixed-bed continuous-flow system (Fig. S2†). The breakthrough curve obtained from the CO₂ adsorption measurements is shown in Fig. 2a, and the CO₂ adsorption amount determined from the breakthrough curve is presented in Fig. 2b. Among Rb-zeolites (such as Rb-13X, Rb-Y, and Rb-beta) and alkali-metal-loaded beta zeolites (such

as Rb-, Na-, K-, and Cs-beta), Rb-beta exhibited the highest amount of CO₂ adsorption. Similarly, we investigated the CO₂ adsorption properties of bare beta zeolite (H-beta) as a reference for comparison with Rb-beta (Fig. S3†). The introduction of Rb⁺ cations increased the CO₂ adsorption capacity, suggesting that the framework oxygen atoms became more electron-rich due to the presence of the basic alkali metal cations.⁴⁵ This result is consistent with previous reports.^{46,47} It is considered that physisorbed CO₂, which interacts weakly with the framework oxygen atoms, was more effectively stabilized within the zeolite structure.

Subsequently, we performed temperature-programmed desorption (TPD) measurements of CO₂ to explore the CO₂ desorption properties of Rb-beta (Fig. 2c). CO₂ desorption from Rb-beta was observed over the temperature range of 50–150 °C, and the total amount of desorbed CO₂ (0.8 mmol g⁻¹) was close to the CO₂ adsorption amount (0.8 mmol g⁻¹). This indicated that adsorbed CO₂ at 50 °C was completely desorbed after heating to 150 °C. To investigate zeolite structure, Fig. S4† shows XRD patterns of alkali-metal-loaded beta zeolite samples. XRD peaks of alkali-metal-loaded beta zeolites closely resembled those of H-beta, indicating that the zeolite framework remained intact after immobilizing alkali metals.

To elucidate the mechanism underlying CO₂ adsorption and desorption, *operando* Fourier transform infrared (FTIR) spectroscopy was performed during the TPD of CO₂ on Rb-beta. A schematic of the setup is shown in Fig. S5†. Prior to the experiment, the infrared (IR) disk was heated under He at 400 °C for 30 min and then cooled to 40 °C. To record the background spectrum, 1% CO₂/He was fed to the sample at 40 °C for 5 min and purged under He. A strong band at 2275 cm⁻¹ assigned to the physically adsorbed CO₂ on zeolite^{48,49} and two weak broad bands at 1720 and 1280 cm⁻¹ assigned to the carbonate species^{50,51} were observed before heating (Fig. 2d). These results indicated that physically adsorbed CO₂ was the main adsorbed species and carbonate was a minor species. As the temperature increased from 60 to 160 °C, the band intensity for the physically adsorbed CO₂ sharply decreased, accompanied by CO₂ formation at the outlet of the IR cell (Fig. 2e). This indicated that the physical adsorption and desorption of CO₂ were responsible for the adsorption/desorption of CO₂ on Rb-beta.

We adopted Ni/CeO₂ and Cu/ZnO/Al₂O₃ as typical catalysts for the methanation and RWGS reactions. The reaction temperatures for these catalysts were optimized by performing steady-state reaction experiments (Fig. 3). When the Ni/CeO₂ catalyst was used, the CO₂ conversion and CH₄ selectivity sharply increased at a temperature of >150 °C (Fig. 3a). The reaction over the temperature range of 200–500 °C resulted in nearly complete conversion of CO₂ to CH₄ (CO₂ conversion ≥97.0%, CH₄ selectivity ≥99.7%). In the case of the RWGS reaction with the Cu/ZnO/Al₂O₃ catalyst, the CO₂ conversion monotonically increased from 2.0% to 78.1% with the temperature over the range of 100–650 °C (Fig. 3b). Compared with equilibrium conversion, the difference of CO₂ conversion was almost zero at 650 °C. Further increasing the

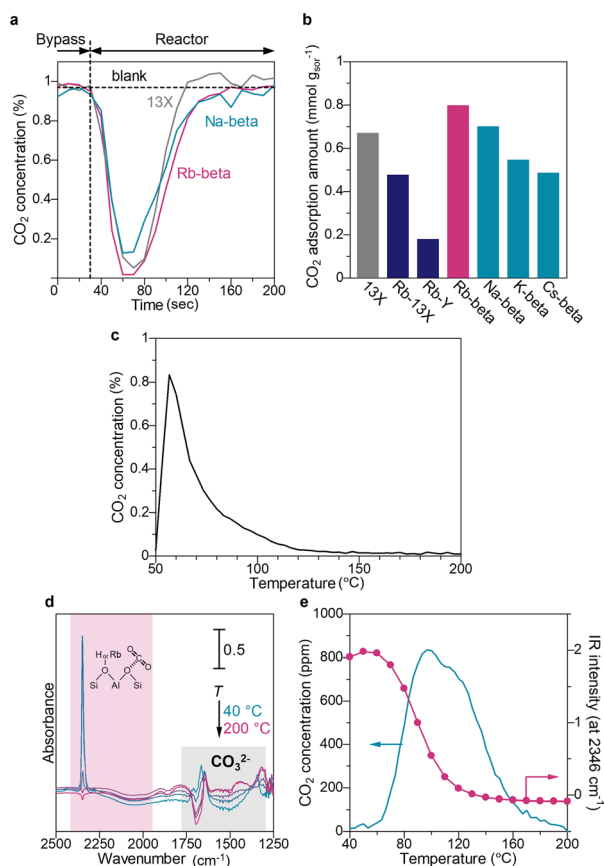


Fig. 2 (a) CO₂ adsorption at 50 °C for 200 s under a flow of 0.97% CO₂ (He balance; total flow: 100 mL min⁻¹). The flow passed through a bypass line in the first 20 s; (b) Comparison between CO₂ adsorption amounts on zeolite sorbents at 50 °C (determined by conducting the experiment shown in Fig. 1a); (c) CO₂ TPD profiles for Rb-beta under He flow. Conditions: heated at 500 °C under He flow and then cooled to 50 °C under He flow; 1% CO₂/N₂ mixture was fed into the reactor at 50 °C for 30 min and purged with He for 5 min. The CO₂ TPD experiment was conducted by applying heat under He flow; (d) *operando* FTIR spectroscopy for Rb-beta under CO₂ TPD condition. IR spectra of adsorbed species at temperature intervals of 40 °C; (e) time-resolved trends in the IR intensities of adsorbed CO₂; concentration of desorbed CO₂. The background spectrum was recorded before CO₂ capture.



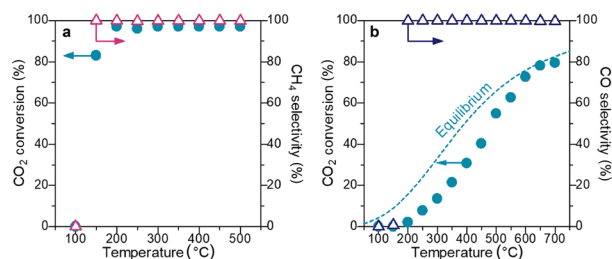


Fig. 3 (a) CO₂ conversion and CH₄ selectivity with respect to reaction temperature with Ni/CeO₂ catalyst; (b) CO₂ conversion and CO selectivity with respect to reaction temperature with Cu/ZnO/Al₂O₃ catalyst. The dependence of the amount of Cu/ZnO/Al₂O₃ is shown in Fig. S6.†

temperature to 700 °C did not significantly improve CO₂ conversion (79.4%). CO selectivity was high ($\geq 99.3\%$) at a temperature of >200 °C.

2.2 Continuous production of O₂-free CO₂ from CO₂ + O₂ mixture

Prior to the continuous CO₂ capture and hydrogenation using the coupled tandem TSA/catalyst system, we demonstrated the continuous production of O₂-free CO₂ from a model combustion exhaust gas (10% CO₂ + 10% O₂/He) using the TSA system. Fig. 4a shows a schematic of the TSA system for O₂-free CO₂ production from the model combustion exhaust gas. Two reactors containing equal amounts of Rb-beta were

set up in parallel for CO₂ capture and desorption. The CO₂ concentrations in effluents 1 and 2 were monitored by performing FTIR spectroscopy, and the O₂ concentration in effluent 1 was monitored by using mass spectrometry (MS). A gas mixture of CO₂ + O₂/He was fed into one reactor for 29.5 min for CO₂ capture and then purged with He (0.5 min) to remove the remaining O₂ from the reactor. The other reactor (containing CO₂-captured Rb-beta) was heated to 200 °C under He to produce O₂-free CO₂ in effluent 2. The details of this procedure are presented in Fig. S7.† Fig. 4b and d show the typical variations in the CO₂ and O₂ concentrations in effluents 1 and 2 over time, respectively. CO₂ is captured from the CO₂/O₂ mixture when the reactor is cooled from 200 to 40 °C. During the CO₂-capture period, the outlet CO₂ concentration (in effluent 1) is below the detection limit, indicating that CO₂ is almost completely removed from the 10% CO₂ + 10% O₂ mixture. Subsequently, two 4-way valves connected to the top and bottom of the tubular reactors are simultaneously switched, and the captured CO₂ is released by heating to 200 °C (5.5 °C min⁻¹) under He flow; this results in the formation of O₂-free CO₂ in effluent 2. The maximum concentration of the liberated CO₂ is ~37%. The amounts of captured CO₂ (12.1 mmol) and produced O₂-free CO₂ (11.9 mmol) in one cycle, calculated by applying eqn (2) and (3) in ESI† Text S3, are shown in Fig. S10 and S11. Note that the production of CO₂ results in an increase in the total flow rate (from 120 to 167 mL min⁻¹) of effluent 2. The CO₂ capture and desorption experiments are performed continuously for

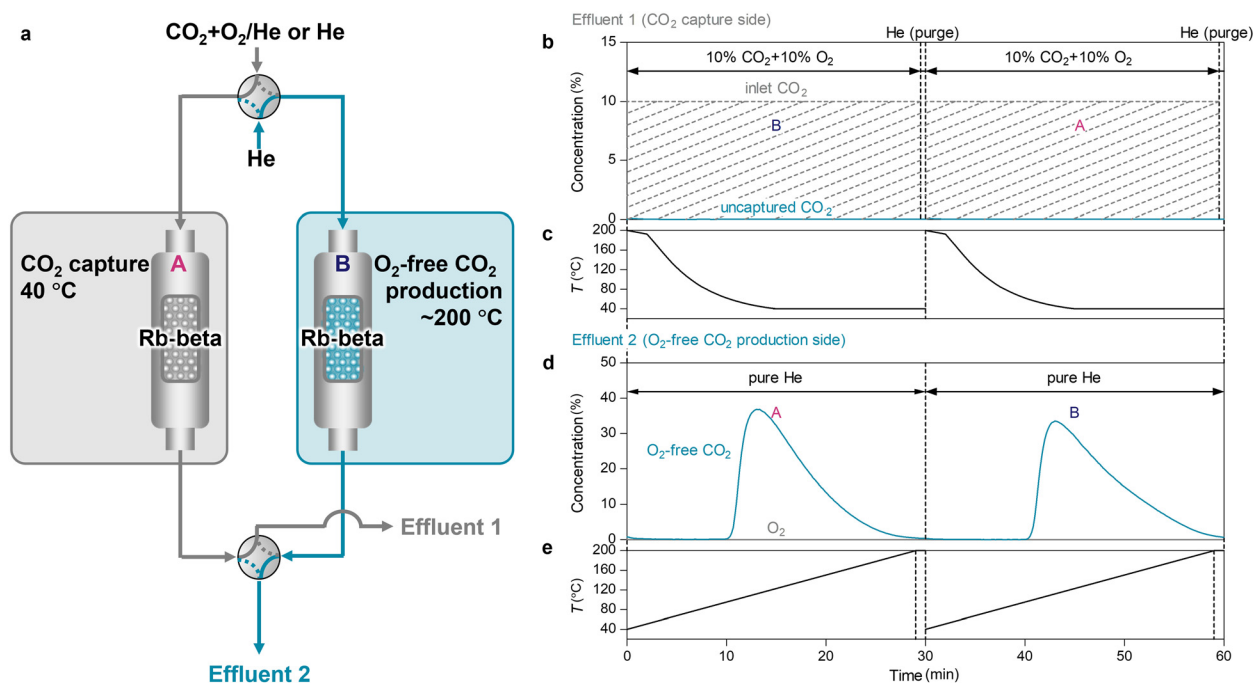


Fig. 4 (a) Schematic of the two-reactor TSA system for continuous CO₂ capture and O₂-free CO₂ production; captured gas (100 mL min⁻¹, 10% CO₂ + 10% O₂/He for 29.5 min and then pure He for 0.5 min) and released gas (120 mL min⁻¹, pure He for 30 min) were alternately fed into each reactor containing 14 g of Rb-beta; (b) and (d) typical variations in the CO₂ and O₂ concentrations in effluents 1 and 2 over time, respectively; (c) and (e) typical temperature changes in reactor A and B over time, respectively. O₂ concentration in effluent 1 is shown in Fig. S8.† The response curves for the outlet CO₂ over the blank are displayed in Fig. S9.†



seven cycles (Fig. S12†). These results clearly reveal the continuous production of O₂-free CO₂ from the 10% CO₂/10% O₂ gas mixture.

2.3 Continuous CO₂ capture and methanation/RWGS reaction using the tandem system

Next, continuous CO₂ capture and methanation were performed using the tandem TSA/methanation system. Unlike DFM designs, the tandem-system design allows individually optimized active sites and reaction conditions for each step. The proposed TSA system converts the model combustion exhaust (10% CO₂ + 10% O₂) to O₂-free CO₂, which undergoes methanation under H₂ in the reactor (containing Ni/CeO₂) downstream at 300 °C (Fig. 5a). Note that H₂ is expected to act as an inert gas, similar to He, because the Rb-beta sorbent does not promote hydrogenation. First, the CO₂ + O₂ mixture is fed into one reactor of the TSA system for 29.5 min for CO₂ capture, and then, pure He (0.5 min) is fed to purge the remaining O₂ in the reactor. The other reactor (containing CO₂-captured Rb-beta) is heated to 200 °C (5.5 °C min⁻¹) under pure H₂ for 30 min. The desorbed CO₂ and H₂ are fed into the methanation reactor and converted to CH₄. The details of this procedure are displayed in Fig. S13.†

Fig. 5b and d show the typical variations in the CH₄, CO₂, and O₂ concentrations in effluents 1 and 2 over time, analyzed online by employing an IR gas-cell and MS, respectively. Fig. 5c and e depict the optimized time

variations in the temperatures of the two TSA reactors. During the CO₂-capture period, the outlet CO₂ concentration (in effluent 1) is below the detection limit, indicating that CO₂ is almost completely removed from the 10% CO₂ + 10% O₂ mixture. Subsequently, two 4-way valves connected to the top and bottom of the tubular reactors are simultaneously switched, and the captured CO₂ is released by heating under H₂. When CO₂-captured Rb-beta is heated under H₂, CH₄ was observed in effluent 2, with a maximum concentration of ~66.3%. The concentration of CO (0.02%) is low, and CO₂ is not present in effluent 2; thus, CH₄ selectivity is ≥99%. Note that the high conversion level of CO₂ and H₂ over the downstream Ni/CeO₂ catalyst results in a significant decrease in the total flow rate (from 120 to 40 mL min⁻¹) of effluent 2 (details on the decrease in the total flow rate are shown in ESI† Text S4 and Fig. S14 and S15). The CO₂ capture and desorption/methanation experiments are performed continuously for four cycles (Fig. S16†). Fig. S17 and S18† show the results of condition optimization for the CO₂ capture and desorption/methanation experiments. The effect of the CO₂-capture temperature (40, 80, 100, and 120 °C) on the CH₄ yield (Fig. S17†) reveals that the lowest temperature (40 °C) produces the highest CH₄ yield, simply because a lower adsorption temperature leads to a larger CO₂ capacity of Rb-beta. The effect of the catalyst amount (Fig. S18†) shows that increasing the catalyst amount (from 2 to 15 g) results in a slight increase in the CH₄ yield (from 85 to 92%) and a large decrease in the space-time-yield of CH₄ (STY_{CH₄}) (from 11.9 to 1.8 mmol g⁻¹ h⁻¹).

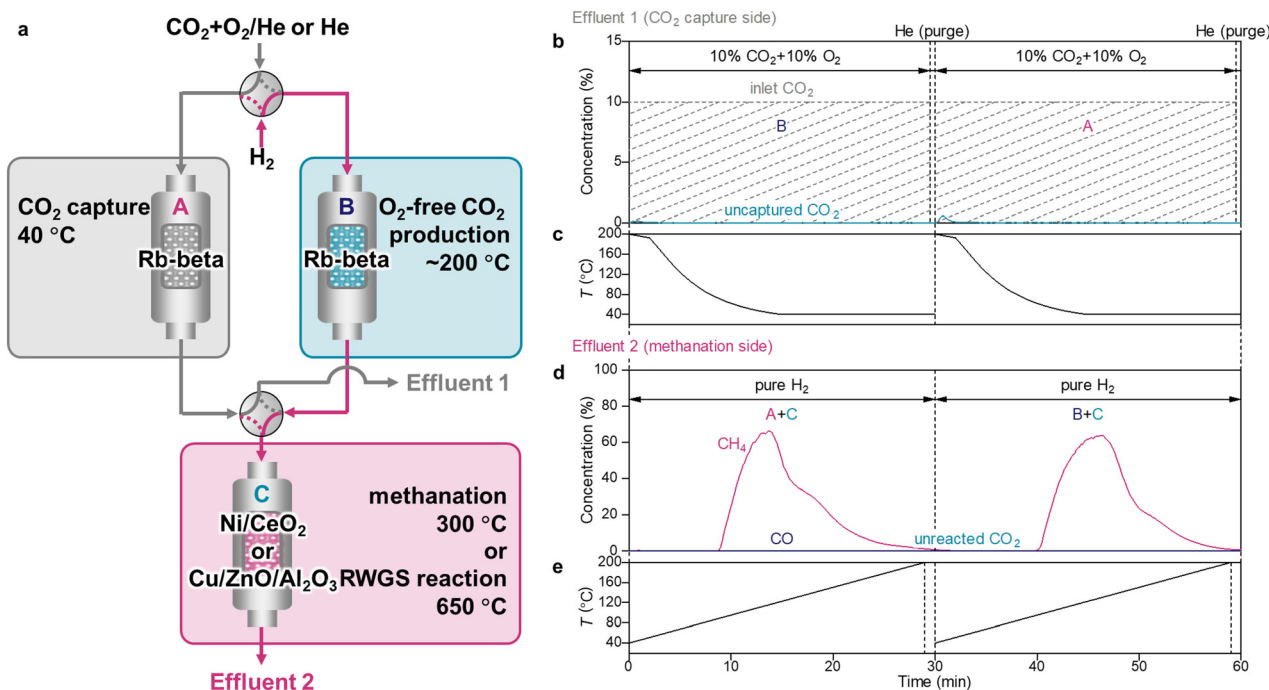


Fig. 5 (a) Schematic of the two-reactor TSA system for continuous CO₂ capture and methanation; captured gas (100 mL min⁻¹; 10% CO₂ + 10% O₂/He for 29.5 min and then pure He for 0.5 min) and hydrogenation gas (120 mL min⁻¹; pure H₂ for 30 min) were alternately fed into each reactor containing 14 g of Rb-beta; (b) and (d) typical variations in the CH₄, CO₂, and CO concentrations in effluents 1 and 2 over time, respectively; (c) and (e) typical temperature changes in reactor A and B over time, respectively.



A CH_4 yield of 92% is almost double those in the previously reported catalytic systems for the methanation of a CO_2/O_2 mixture using CCR (16 reports and 55 reaction processes presented in Fig. 6a; details are listed in Table S1†). The reaction temperature in our system (300 °C) is the lowest among the reported systems, and the inlet CO_2 concentration in our system is the highest among the reported systems. Note that the majority of the previously reported CCR systems for CH_4 production were tested in the absence of O_2 during the CO_2 -capture period (10 reports and 100 reaction processes; details are listed in Table S2†). Compared with those systems, our system produces the highest CH_4 yield.

Under conditions relevant to future practical implementation, gas purging with unreacted gas is expected to be avoided, and recycling of unreacted H_2 is anticipated to be implemented. Continuous CO_2 capture and methanation were conducted using the tandem system without gas purging (Fig. S19†). Under these conditions, the effluent gas composition remained nearly unchanged compared to that observed under gas purge conditions (Fig. 5d), suggesting that the effect of transient O_2 inflow was negligible. This is possibly because oxidized Ni species were readily reduced during the initial introduction of H_2 , demonstrating that this tandem system exhibits complete O_2 -tolerance. While the current system shows high performance, future implementation of CH_4/H_2 product gas recycling as a reductive gas suggests the potential to further improve H_2 utilization efficiency.

We demonstrated continuous CO_2 capture and the RWGS reaction using a system similar to that described in the previous subsection; in this system, a commercial $\text{Cu}/\text{ZnO}/\text{Al}_2\text{O}_3$ catalyst was used as the RWGS catalyst (catalyst amount = 10 g) (Fig. S20†). When Rb-beta was heated from 40 to 200 °C, CO was formed with a maximum concentration of ~41.0%, CO_2 was desorbed with a maximum concentration of ~11.2%, and almost no CH_4 was detected (CO selectivity $\geq 99\%$). In addition, no CO_2 was detected in effluent 1 using gas-cell IR, indicating that almost all the supplied CO_2 was captured by Rb-beta. Given the CO production per unit time (a detailed explanation is presented in ESI† Text S5 and Fig. S21), the conversion of inlet CO_2 to CO (denoted as the CO yield) was 85%, indicating that a

considerable amount of the supplied high-concentration CO_2 in the presence of O_2 was continuously converted to CO. This reaction was repeated several times and maintained for at least 2 h (six cycles; Fig. S22†). Furthermore, the amount of $\text{Cu}/\text{ZnO}/\text{Al}_2\text{O}_3$ included in this RWGS system was optimized from 0.2 to 14 g (Fig. S23†). When the catalyst amount was between 1 to 15 g, the CO yield was over 85% and the maximum CO production rate was $20.1 \text{ mmol g}^{-1} \text{ h}^{-1}$. When the catalyst amount was decreased to 0.2 g, the CO yield decreased by 45% but the space-time-yield of CO (STY_{CO}) increased to $55.5 \text{ mmol g}^{-1} \text{ h}^{-1}$. Thus, increasing the catalyst amount from 0.2 to 1 g resulted in a sharp increase in the CO yield (from 45% to 85%), but further increasing the amount from 1 to 15 g resulted in limited change (from 85% to 81%). Additionally, increasing the catalyst amount from 0.2 to 15 g significantly decreased the STY_{CO} from 55.5 to $1.5 \text{ mmol g}^{-1} \text{ h}^{-1}$.

The system was compared with previously reported systems (10 reports and 30 reaction processes in Fig. 6b; details are listed in Table S3†). The majority of the previously reported CCR systems for CO production were evaluated at low inlet CO_2 concentrations (below 1%). Our system demonstrated the RWGS process with a high CO yield (85%) at a high inlet CO_2 concentration (10%). Notably, many of the previously studied CCR systems aimed at CO production were tested in the absence of O_2 during CO_2 capture (as detailed in Table S4;† 10 reports and 100 reaction processes). Compared with systems with the same inlet CO_2 concentration (10%), our system demonstrated approximately twice the CO yield.

For example, in Fischer-Tropsch (FT),⁵² methanol (MeOH),⁵³ and ethanol (EtOH) syntheses⁵⁴ from syngas, the H_2/CO ratio of the syngas significantly affects the selectivity and yield of the product. Similar to the aforementioned methanation system, the H_2 input was optimized (Fig. 7). When the H_2 flow time was reduced from 30 to 20 min in one cycle, the H_2 conversion slightly increased from 9.8% to 15% and the H_2/CO ratio changed from 9.1 to 3.7, which is closer to the ideal value of 2.0 for FT, MeOH, and EtOH syntheses, while retaining a high CO yield (93%) (see ESI† Text S5 for details). Furthermore, syngas is an environment-friendly alternative gaseous fuel for internal combustion during engine operations, and H_2 -rich syngas ($\text{H}_2/\text{CO} \geq 3.0$) has been reported to improve thermal efficiency;⁵⁵ this continuous RWGS process also has the potential to provide industrially valuable syngas. This technique is effective for continuous CO_2 capture and methanation. A decrease in the H_2 flow time improved the H_2 utilization efficiency (H_2 conversion increased from 38% to 58%; Fig. S24; see ESI† Text S6 for details).

In this chapter, we demonstrated that the developed tandem system is effective for the ambient-pressure conversion of CO_2 in model combustion exhaust into CH_4 and CO *via* methanation and RWGS reaction. Because this system does not require a pressure swing adsorption (PSA) unit, it has the potential to operate all reactors under

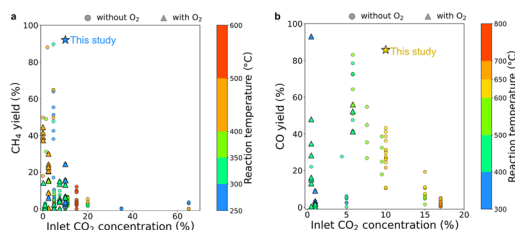


Fig. 6 Performance of (a) methanation and (b) RWGS reaction processes in the proposed system and previously reported systems for exhaust or atmospheric CO_2 conversion (references are listed in Tables S1–S4†).



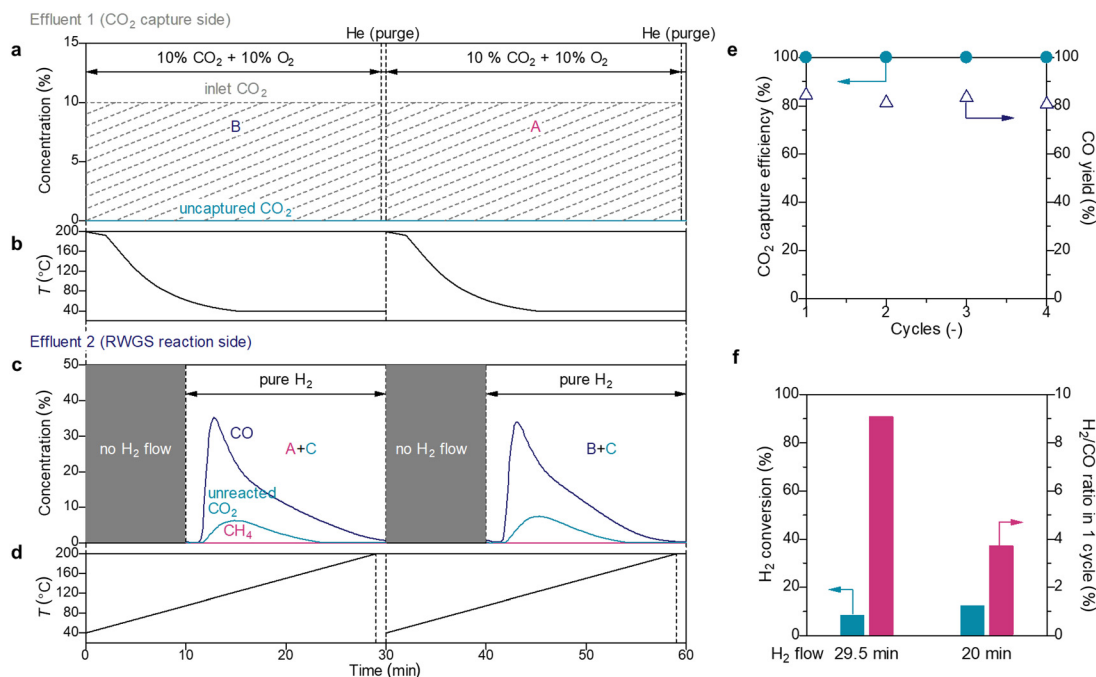


Fig. 7 Continuous CO₂ capture and methanation; captured gas (100 mL min⁻¹; 10% CO₂ + 10% O₂/He for 29.5 min and then pure He for 0.5 min) and hydrogenation gas (120 mL min⁻¹; pure H₂ for 20 min) were alternately fed into each reactor containing 14 g of Rb-beta. (a) and (c) typical variations in the CH₄, CO₂, and CO concentrations in effluents 1 and 2 over time, respectively; (b) and (d) typical temperature changes in reactors a and b over time, respectively; (e) changes in the CO₂ capture efficiency and CO yield during cyclic test; (f) comparison of H₂ conversion and ratio of effluent CO to H₂ in one cycle between the conditions depicted in Fig. S20a† (H₂ flow for 29.5 min) and those in Fig. 7a (H₂ flow for 20 min).

uniform pressurized conditions. This tandem system with conventional MeOH or FT synthesis catalysts such as Cu/ZnO/Al₂O₃^{56–58} and Fe-based catalysts,^{59,60} which operate under elevated pressure, could enable the direct synthesis of methanol and liquefied petroleum gas (LPG) from CO₂ in model combustion exhaust streams.

2.4 Continuous direct air capture and methanation

Next, we broadened the applicability of the proposed system for continuous CH₄ production from ambient CO₂ (Fig. 8).

For ambient CO₂ capture and methanation, a high flow rate (500 mL min⁻¹) of air was fed into one TSA reactor for 60 min, whereas a low flow rate (10 mL min⁻¹) of pure H₂ was fed to the other TSA reactor (containing CO₂-captured Rb-beta) for 60 min. The H₂ and desorbed CO₂ from the other TSA reactor were subsequently fed into the downstream methanation reactor (containing Ni/CeO₂). When CO₂-captured Rb-beta was heated under H₂, the desorbed CO₂ underwent methanation on the downstream Ni/CeO₂ catalyst to produce a high concentration of CH₄. The maximum CH₄ concentration was 0.7%, and the average CH₄ concentration

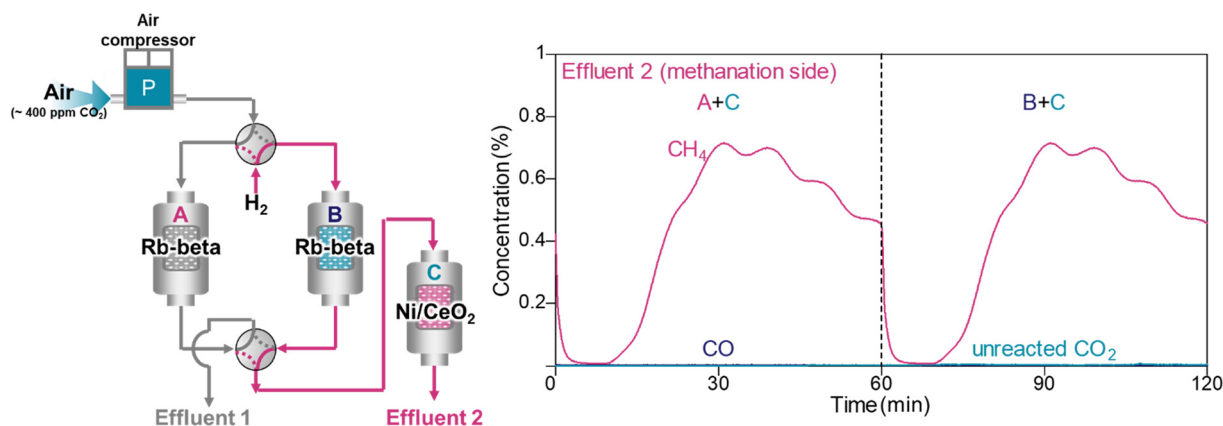


Fig. 8 Schematic and typical variations in the CH₄, CO, and unreacted CO₂ amounts in effluent 2 over time for continuous direct air capture and methanation. Conditions: 14 g of Rb-beta for each upper reactor and temperature swing from 40 to 200 °C (heating rate = 20 °C min⁻¹); 15 g of Ni/CeO₂ for the bottom reactor, 300 °C, and 500 mL min⁻¹ air for 60 min and switched to 10 mL min⁻¹ H₂ for another 60 min.

was ~0.4%. The results highlight the production of 10 times enriched CH₄ from atmospheric CO₂. As shown in our previous study,⁶¹ the enrichment methodology is simply based on the difference in the flow rates for CO₂ capture (500 mL min⁻¹) and reduction (10 mL min⁻¹). As shown in Fig. S25,† the proposed methanation method is also applicable to high concentrations (40%) of CO₂. The 40% CO₂ + 10% O₂ mixture undergoes methanation, and the CH₄ yield is ~70%. These results demonstrate that the proposed methanation system can be applied to a wide range of CO₂ concentrations.

2.5 Energy efficiency

To assess the energy requirements of the two processes, we analyzed the energy efficiency (η) and fuel production efficiency (FPE) of the tandem methanation and CCR systems.⁶² The η for CO₂ conversion reactions was calculated using the following equation:⁶³

$$\eta (\%) = \frac{\Delta H_R (\text{kJ mol}^{-1}) \cdot X_{\text{CO}_2} \cdot r_{\text{CO}_2, \text{in}} (\text{mol s}^{-1})}{P (\text{kW})},$$

where $r_{\text{CO}_2, \text{in}}$ represents the molar flow rate of CO₂ at the inlet of the reactor, and ΔH_R is the reaction enthalpy (-165 kJ mol⁻¹ for the methanation process at 298 K). The calculated η values for the two systems are plotted as a function of time elapsed in Fig. 9a. The η for CCR is 46% at the beginning of the reaction but declines exponentially owing to the limited CO₂ capacity of the DFM. In contrast, the η for tandem methanation is significantly higher than that for CCR, owing to the lower total thermal input and greater CH₄ production. The system performances are compared in Fig. 9b. The advantages of tandem methanation over CCR are evident in terms of the CH₄ yield, CH₄ selectivity, CH₄ production per

gram of the catalyst + adsorbent (to ensure a fair comparison between the two systems), and η . Note that the η for tandem methanation exceeds 100%. This is because only the power input is considered in the overall energy input and output and the net energy flow of the reactants and products is ignored.

We also compared the FPEs of the two systems. The FPE for the methanation reaction is defined as the ratio of the energy output in the form of methane (not considering unreacted H₂ at the exit) to the total energy input. The output energy is estimated based solely on the low heating value of CH₄ (LHV_{CH₄}), because the condensation heat of the produced water is typically not recovered. The energy input includes both the thermal input and the feed gas (H₂), which possesses a heating value and contributes energy to the process. Therefore, the FPE is calculated as

$$\begin{aligned} \text{FPE} (\%) &= \frac{\text{Output energy}}{\text{Input energy}} \\ &= \frac{\text{LHV}_{\text{CH}_4} (\text{kJ mol}^{-1}) \cdot r_{\text{CH}_4} (\text{mol s}^{-1})}{P (\text{kW}) + \text{LHV}_{\text{H}_2} (\text{kJ mol}^{-1}) \times (r_{\text{H}_2, \text{in}} - r_{\text{H}_2, \text{out}}) (\text{mol s}^{-1})} \end{aligned}$$

where P is the thermal input, r_{CH_4} is the mole of CH₄ production, $r_{\text{H}_2, \text{in}} - r_{\text{H}_2, \text{out}} = (n_{\text{H}_2, \text{in}} - n_{\text{H}_2, \text{out}})/\Delta t$ is the rate of H₂ consumption, and LHV_{H₂} and LHV_{CH₄} are the LHV's of the converted hydrogen and methane (242 and 801 kJ mol⁻¹), respectively. As depicted in Fig. 9b, tandem methanation yields a high FPE of 83%, whereas CCR exhibits an FPE of 80%.

3 Conclusions

In summary, we developed a new method for the continuous production of O₂-free CO₂, CH₄, and CO from the atmosphere and a simulated exhaust gas (CO₂/O₂/He mixture). The

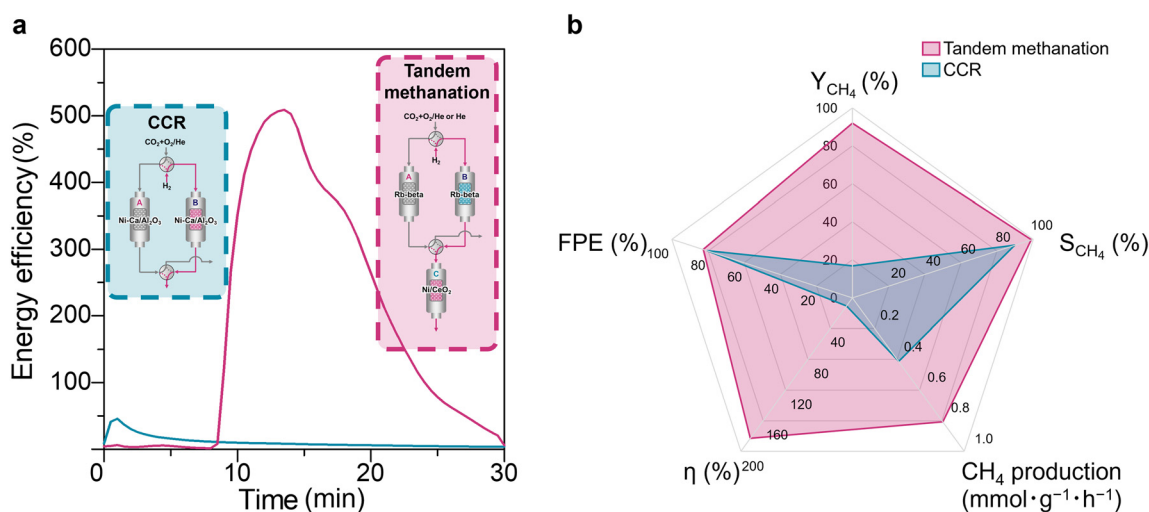


Fig. 9 (a) Typical variations in the energy efficiencies of CCR and tandem methanation system over time. Conditions: 14 g of Rb-beta for each upper reactor and temperature swing from 40 to 200 °C (heating rate = 20 °C min⁻¹); 15 g of Ni/CeO₂ for the bottom reactor, 300 °C, and 500 mL min⁻¹ air for 60 min and switched to 10 mL min⁻¹ H₂ for another 60 min; (b) comparison of the CH₄ yield (Y_{CH_4}), CH₄ selectivity (S_{CH_4}), CH₄ production, energy efficiency (η), and fuel production efficiency (FPE) between the CCR and tandem methanation system. Parameters explaining energy efficiency, such as η and FPE, are detailed in ESI† Text S7.



developed process is suitable for continuous operation over a low-temperature swing of 40–200 °C on a Rb-beta sorbent combined with a methanation system at 300 °C and a RWGS system (for syngas synthesis) at 650 °C. The results of this study revealed that the developed process is almost twice as effective as CCR for CO₂ capture and hydrogenation. We also provided evidence that the energy efficiency of the tandem methanation process based on the overall energy input and output is comparatively high because of the low power input required to operate the system and the high CH₄ production. This approach is promising for CO₂ utilization *via* direct air and post-combustion gas capture and conversion to green fuels. In the future, we expect that our flexible process, in combination with efficient catalysts, will contribute to a carbon-neutral society.

4 Methods

4.1 Sorbent and catalyst preparation

Beta (Si/Al = 5, Mitsui Mining & Smelting Co., Ltd.), 13X (Si/Al = 1.25, Junsei Chemical Co., Ltd.), and Na-Y zeolites (Si/Al = 2.75, JRC-Z-Y5.5, Tosoh Corporation) were used as sorbents and supports. To prepare Rb-loaded zeolite sorbents, Rb species were immobilized on the zeolites using the conventional impregnation method. An appropriate amount of a Rb₂CO₃ aqueous solution (AR > 99%, FUJIFILM WAKO Pure Chemical Corporation) was incorporated into the zeolites. After being stirred for 3 h at 25 °C, the suspension was evaporated by using a vacuum pump at 50 °C and dried overnight at 100 °C. The solid produced was then calcined at 200 °C for 1 h to obtain the desired Rb-zeolites. Other alkali-metal-loaded zeolite sorbents were prepared by employing the same approach using K₂CO₃ (AR: 99.0%, Tokyo Chemical Industry Co., Ltd.) and Cs₂CO₃ (AR > 99%, FUJIFILM WAKO Pure Chemical Corporation) as precursors.

4.2 Characterization

CO₂ adsorption measurements were performed by using a fixed-bed flow reactor (Fig. S1†). The zeolite sorbents (50 mg) were placed on quartz wool in the middle of a reactor, which was then placed in an electric tube furnace. The zeolite sorbents were heated to 500 °C under pure He flow (100 mL min⁻¹), maintained for 30 min to remove the CO₂ and water vapor included in the zeolites, and cooled to 40 °C. The gas emitted from the reactor outlet was directly connected to a homemade IR gas cell to monitor the CO₂ concentration by performing IR measurements. In the first 30 s, before the CO₂ concentration stabilized, a flow of 1% CO₂/He was passed through the bypass line and then the feed was switched to the reactor. The CO₂ adsorption amount was calculated from the difference in CO₂ concentrations between the blank and zeolites. Due to the high absorbance of CO₂ in gas-cell IR measurements, fluctuations in the ambient CO₂ concentration can lead to slight variations in the measured values. To evaluate the reproducibility, each sample was measured three times. The resulting deviation in CO₂

concentration was within approximately ±0.05%, corresponding to an error margin of about ±0.04 mmol g_{sor}⁻¹ in the calculated CO₂ adsorption amount. The TPD of CO₂ was also performed using the homemade IR gas cell. The zeolite (100 mg) was pretreated in He atmosphere at 500 °C for 30 min and then cooled to 50 °C. Next, the 1% CO₂/N₂ (100 mL min⁻¹) mixed gas was fed into the reactor for 30 min and then He was flowed for 15 min. The TPD profile was obtained by heating the sample from 30 to 200 °C at a rate of 20 °C min⁻¹ under He flow. *Operando* FTIR measurements were performed during the TPD of CO₂ using a JASCO FT/IR-4600 spectrometer equipped with a mercury-cadmium-telluride detector and a flow-type quartz IR cell connected to a flow system (total flow rate = 100 mL min⁻¹; Fig. S2†). The effluent gas was simultaneously monitored by performing FTIR spectroscopy (JASCO FT/IR-4600) using a homemade gas cell. A sample pellet (40 mg; diameter: 20 mm) was introduced into a quartz cell equipped with a CaF window. The sample pellet was pretreated at 200 °C for 30 min under He flow and cooled to 40 °C, and the 1% CO₂/He mixture was fed into the reactor for 5 min. Subsequently, the system was purged with He for 10 min and the background spectrum was recorded. Temperature-resolved measurements were performed from 40 to 200 °C. The *operando* IR measurements were performed by monitoring the desorption of CO₂ in the outlet gas mixture.

4.3 Continuous CO₂ capture and O₂-free CO₂ production using two parallel reactors

Continuous CO₂ capture and O₂-free CO₂ production were performed using a system similar to that in a previous study.⁶¹ CO₂ was continuously separated by using two fixed-bed flow reactors (Fig. S7†), and the response curves for CO₂ were obtained using a blank test (Fig. S9†). Two vertical quartz reactors (A and B) containing the same sorbent powder (14 g) were placed on quartz wool in the middle of the reactor in an electric tube furnace. The sorbents were pretreated under pure He flow (100 mL min⁻¹) at 400 °C. Subsequently, continuous CO₂ capture and O₂-free CO₂ production were achieved. Two timer-controlled 4-way valves were switched simultaneously to feed a simulated exhaust gas (100 mL min⁻¹; 10% CO₂ + 10% O₂/He for 29.5 min and He for 0.5 min) and an O₂-free CO₂ gas (120 mL min⁻¹; He for 30 min); when the simulated exhaust gas was fed to reactor A, the O₂-free CO₂ gas was fed to reactor B. Effluent gases containing uncaptured CO₂ from reactor A and B (with O₂ and He) were continuously fed into effluent 1. The produced O₂-free CO₂ in reactors A and B (with He) was continuously fed into effluent 2. The effluent gas was simultaneously monitored by performing FTIR spectroscopy (JASCO FT/IR-4600) using a gas cell and a mass spectrometer (BELMass, MicrotracBEL Corp.). The CO₂ concentration was calculated using the calibration curve for the CO₂ concentration and the IR peak area in the range of 2395–2235 cm⁻¹ for ≤1% CO₂ and 3760–3662 cm⁻¹ for >1% CO₂. The CO₂ capture efficiency and the yield of O₂-free CO₂ were calculated as follows:



$$\text{CO}_2 \text{ capture efficiency } [\%] = \frac{\int_0^t [F_{\text{CO}_2}^{\text{in}} - F_{\text{CO}_2}^{\text{out}(1)}(t)] dt}{\int_0^t F_{\text{CO}_2}^{\text{in}}(t) dt} \times 100;$$

$$\text{Yield of O}_2 \text{ free CO}_2 [\%] = \frac{\int_0^t F_{\text{CO}_2}^{\text{out}(2)}(t) dt}{\int_0^t F_{\text{CO}_2}^{\text{in}}(t) dt} \times 100,$$

where $F_{\text{CO}_2}^{\text{in}}$, $F_{\text{CO}_2}^{\text{out}(1)}$, and $F_{\text{CO}_2}^{\text{out}(2)}$ are the CO_2 molar flow rates at the column inlet and the outlets of effluents 1 and 2, respectively, and t denotes the duration of one cycle.

4.4 Continuous CO_2 capture and methanation/RWGS reaction using the combined system with two parallel reactors for TSA and a single reactor for hydrogenation

Continuous CO_2 capture and hydrogenation (such as the methanation and RWGS reactions) were performed using homemade reactors (Fig. 1c; detailed procedure is shown in Fig. S13†). Two vertical quartz reactors (A and B) containing the Rb-beta sorbent powder (14 g), same as those used for O_2 -free CO_2 production, were placed on quartz wool in the middle of the reactor in an electric tube furnace. For the methanation and RWGS reactions, Ni/CeO₂ and Cu/ZnO/Al₂O₃ (commercial, Alfa Aesar) were added to the bottom reactor (C). The sorbents were pretreated under He flow for 30 min at 400 °C. Ni/CeO₂ was pretreated with H_2 for 30 min at 400 °C. Cu/ZnO/Al₂O₃ was pretreated with H_2 for 30 min at 500 °C. After these pretreatments, continuous CO_2 capture and hydrogenation were performed. Similar to the continuous O_2 -free CO_2 production system, 1% CO_2 + 10% O_2 /He or pure He (for purging) and pure H_2 were alternately flowed to each Rb-beta under cooling and heating. The produced O_2 -free CO_2 and H_2 were fed into a hydrogenation catalyst (in reactor C). Effluent 1 contained the uncaptured CO_2 , O_2 , and He. Effluent 2 contained the produced CH_4 , CO, and unreacted CO_2 . The produced H_2O was trapped before the gas concentrations were analyzed using cold trap equipment. The gas compositions in effluents 1 and 2 (CO_2 , CO, and CH_4) were analyzed online by using an FTIR spectrometer (JASCO FT/IR-4600) with a gas cell. The STY_{CH_4} , STY_{CO} , CH_4 , and CO yields and H_2 conversion are calculated as follows:

$$\text{STY}_{\text{CH}_4} \text{ or } \text{STY}_{\text{CO}} [\text{mmol g}^{-1} \text{ h}^{-1}] = \frac{\int_0^t F_{\text{CH}_4 \text{ or CO}}^{\text{out}}(t) dt}{m_{\text{cat}} \times t};$$

$$\text{CH}_4 \text{ or CO yield } [\%] = \frac{\int_0^t F_{\text{CH}_4 \text{ or CO}}^{\text{out}}(t) dt}{\int_0^t F_{\text{CO}_2}^{\text{in}}(t) dt} \times 100,$$

$$\text{H}_2 \text{ conversion } [\%] = \frac{\int_0^t F_{\text{CO}}^{\text{out}}(t) dt + 4 \int_0^t F_{\text{CH}_4}^{\text{out}}(t) dt}{\int_0^t F_{\text{H}_2}^{\text{in}}(t) dt} \times 100$$

where $F_{\text{CH}_4}^{\text{out}}$ and $F_{\text{CO}}^{\text{out}}$ are the CH_4 and CO molar flow rates, respectively, at the column outlet of effluent 2, $F_{\text{CO}_2}^{\text{in}}$ and $F_{\text{H}_2}^{\text{in}}$ are the CO_2 and H_2 molar flow rates at the column inlet, and m_{cat} is the catalyst mass. H_2 conversion was calculated based

on the stoichiometric consumption primarily associated with the formation of CO and CH_4 . To determine the CO and CH_4 molar flow rates, the peak area values around 2250–2001 and 3031–2994 cm^{-1} were used, respectively. The power consumption (P) for reactor heating, which represents the thermal input, was measured using an electrical power consumption analyser (ELPA, EC-05EB).

4.5 Continuous CCR to CH_4 system

Continuous CO_2 capture and reduction to CH_4 using the combined two parallel reactors were performed using homemade reactors (Fig. S14†). Two vertical quartz reactors (A and B), each containing the Ni-Ca/Al₂O₃ sieves, were placed on quartz wool in the middle of an electric tube furnace. Each Ni-Ca/Al₂O₃ was pretreated with H_2 for 30 min at 500 °C. After these pretreatments, continuous CCR was performed. 1% CO_2 + 10% O_2 /He and pure H_2 were alternately flowed to each Ni-Ca/Al₂O₃ under isothermal conditions. Effluent 1 contained the uncaptured CO_2 , O_2 , and He. Effluent 2 contained the produced CH_4 , CO, and unreacted CO_2 . The produced H_2O was trapped before the gas concentrations were analyzed using cold trap equipment. The gas compositions in effluents 1 and 2 (CO_2 , CO, and CH_4) were analyzed online by using an FTIR spectrometer (JASCO FT/IR-4600) with a gas cell.

Data availability

The data that support the findings of this study are available from the corresponding author upon reasonable request.

Author contributions

S. Miy. wrote the manuscript draft and conducted the majority of the experiments, including validation and methodology development (writing – original draft, investigation, validation, methodology). A. A. supervised the project and contributed to manuscript revision (supervision, writing – review & editing). Y. M. and H. S. F. assisted with catalyst preparation and performed catalytic activity trials (investigation, validation). S. Min. and T. T. provided valuable insights into the experimental work and contributed to data visualization and manuscript revision (visualization, writing – review & editing). K. S. designed and supervised the overall project and secured funding (supervision, conceptualization, writing – review & editing, funding acquisition).

Conflicts of interest

There are no conflicts to declare.

Acknowledgements

This study was supported by the “Moonshot Research and Development Program” (JPNP18016), commissioned by the New Energy and Industrial Technology Development Organization (NEDO), KAKENHI (23K20034,



and 21H04626) from the Japan Society for the Promotion of Science (JSPS) and the Joint Usage/Research Center for Catalysis. S. Miy. acknowledges the Grant-in-Aid for JSPS Fellows (24KJ0267, DC2).

References

- 1 D. A. Lashof and D. R. Ahuja, Relative contributions of greenhouse gas emissions to global warming, *Nature*, 1990, **344**, 529–531.
- 2 E. S. Sanz-Pérez, C. R. Murdock, S. A. Didas and C. W. Jones, Direct capture of CO₂ from ambient air, *Chem. Rev.*, 2016, **116**, 11840–11876.
- 3 C. F. Schleussner, J. Rogelj, M. Schaeffer, T. Lissner, R. Licker, E. M. Fischer, R. Knutti, A. Levermann, K. Frieler and W. Hare, Science and policy characteristics of the Paris Agreement temperature goal, *Nat. Clim. Change*, 2016, **6**, 827–835.
- 4 S. Fawzy, A. I. Osman, J. Doran and D. W. Rooney, Strategies for mitigation of climate change: A review, *Environ. Chem. Lett.*, 2020, **18**, 2069–2094.
- 5 M. Tamura, M. Honda, Y. Nakagawa and K. Tomishige, Direct conversion of CO₂ with diols, aminoalcohols and diamines to cyclic carbonates, cyclic carbamates and cyclic ureas using heterogeneous catalysts, *J. Chem. Technol. Biotechnol.*, 2014, **89**, 19–33.
- 6 A. Álvarez, A. Bansode, A. Urakawa, A. V. Bavykina, T. A. Wezendonk, M. Makkee, J. Gascon and F. Kapteijn, Challenges in the greener production of formates/formic acid, methanol, and DME by heterogeneously catalyzed CO₂ hydrogenation processes, *Chem. Rev.*, 2017, **117**, 9804–9838.
- 7 International Energy Agency, *The Future of Hydrogen: Seizing Today's Opportunities*, IEA, Paris, 2019.
- 8 C. Gough, Carbon capture and storage: A review of the global status, *Int. J. Greenhouse Gas Control*, 2008, **2**, 155–168.
- 9 S. Kammerer, I. Borho, J. Jung and M. S. Schmidt, Review: CO₂ capturing methods of the last two decades, *Int. J. Environ. Sci. Technol.*, 2023, **20**, 8087–8104.
- 10 H. A. Patel, J. Byun and C. T. Yavuz, Carbon dioxide capture adsorbents: Chemistry and methods, *ChemSusChem*, 2017, **10**, 1303–1317.
- 11 I. S. Omodolor, H. O. Otor, J. A. Andonegui, B. J. Allen and A. C. Alba-Rubio, Dual-function materials for CO₂ capture and conversion: A review, *Ind. Eng. Chem. Res.*, 2020, **59**, 17612–17631.
- 12 B. Shao, Y. Zhang, Z. Sun, J. Li, Z. Gao, Z. Xie, J. Hu and H. Liu, CO₂ capture and in-situ conversion: recent progresses and perspectives, *Green Chem. Eng.*, 2022, **3**, 189–198.
- 13 L. F. Bobadilla, J. M. Riesco-García, G. Penelás-Pérez and A. Urakawa, Enabling continuous capture and catalytic conversion of flue gas CO₂ to syngas in one process, *J. CO₂ Util.*, 2016, **14**, 106–111.
- 14 M. S. Duyar, M. A. A. Treviño and R. J. Farrauto, Dual function materials for CO₂ capture and conversion using renewable H₂, *Appl. Catal., B*, 2015, **168–169**, 370–376.
- 15 F. Kosaka, Y. Liu, S. Y. Chen, T. Mochizuki, H. Takagi, A. Urakawa and K. Kuramoto, Enhanced activity of integrated CO₂ capture and reduction to CH₄ under pressurized conditions toward atmospheric CO₂ utilization, *ACS Sustainable Chem. Eng.*, 2021, **9**, 3452–3463.
- 16 M. Sakai, H. Imagawa and N. Baba, Layered-double-hydroxide-based Ni catalyst for CO₂ capture and methanation, *Appl. Catal., A*, 2022, **647**, 118904.
- 17 L. Li, S. Miyazaki, Z. Wu, T. Toyao, R. Selyanchyn, Z. Maeno, S. Fujikawa and K. Shimizu, Continuous direct air capture and methanation using combined system of membrane-based CO₂ capture and Ni-Ca based dual functional materials, *Appl. Catal., B*, 2023, **339**, 123151.
- 18 L. Li, Z. Wu, S. Miyazaki, T. Toyao, Z. Maeno and K. Shimizu, Continuous CO₂ capture and methanation over Ni-Ca/Al₂O₃ dual functional materials, *RSC Adv.*, 2023, **13**, 2213–2219.
- 19 S. Miyazaki, L. Li, S. Yasumura, K. W. Ting, T. Toyao, Z. Maeno and K. Shimizu, Continuous CO₂ capture and selective hydrogenation to CO over Na-promoted Pt nanoparticles on Al₂O₃, *ACS Catal.*, 2022, **12**, 2639–2650.
- 20 L. Li, N. Zhang, Z. Wu, S. Miyazaki, T. Toyao, Z. Maeno and K. Shimizu, Rb-Ni/Al₂O₃ as dual functional material for continuous CO₂ capture and selective hydrogenation to CO, *Chem. Eng. J.*, 2023, **477**, 147199.
- 21 B. Lu, Y. Fan, X. Zhi, Z. Han, F. Wu, X. Li, C. Luo and L. Zhang, Material design and prospect of dual-functional materials for integrated carbon dioxide capture and conversion, *Carbon Capture Sci. Technol.*, 2024, **12**, 100207.
- 22 M. T. Dunstan, F. Donat, A. H. Bork, C. P. Grey and C. R. Müller, CO₂ Capture at medium to high temperature using solid oxide-based sorbents: fundamental aspects, mechanistic insights, and recent advances, *Chem. Rev.*, 2021, **121**, 12681–12745.
- 23 K. T. Leperi, D. Yancy-Caballero, R. Q. Snurr and F. You, 110th anniversary: Surrogate models based on artificial neural networks to simulate and optimize pressure swing adsorption cycles for CO₂ capture, *Ind. Eng. Chem. Res.*, 2019, **58**, 18241–18252.
- 24 M. Krödel, A. Landuyt, P. M. Abdala and C. R. Müller, Mechanistic understanding of CaO-based sorbents for high-temperature CO₂ capture: Advanced characterization and prospects, *ChemSusChem*, 2020, **13**, 6259–6272.
- 25 S. Miyazaki, D. Chen, B. Jiacheng, T. Toyao, Y. Kanda and K. Shimizu, *In situ* spectroscopic study of CO₂ capture and methanation over Ni-Ca based dual functional materials, *Chem. – Asian J.*, 2024, **19**, e202301003.
- 26 Z. Tao, Y. Tian, W. Wu, Z. Liu, W. Fu, C.-W. Kung and J. Shang, Development of zeolite adsorbents for CO₂ separation in achieving carbon neutrality, *npj Mater. Sustain.*, 2024, **2**, 20.
- 27 D. G. Boer, J. Langerak and P. P. Pescarmona, Zeolites as selective adsorbents for CO₂ separation, *ACS Appl. Energy Mater.*, 2023, **6**, 2634–2656.
- 28 G. Shah, E. Ahmad, K. K. Pant and V. K. Vijay, Comprehending the contemporary state of art in biogas



- enrichment and CO₂ capture technologies via swing adsorption, *Int. J. Hydrogen Energy*, 2021, **46**, 6588–6612.
- 29 Q. Ma, J. Li, Y. Li and J. Choi, Recent progress and issues facing zeolite and metal-organic framework membranes: From membrane synthesis to applications, *J. Membr. Sci.*, 2024, **690**, 122201.
 - 30 N. Rangnekar, N. Mittal, B. Elyassi, J. Caro and M. Tsapatsis, Zeolite membranes – a review and comparison with MOFs, *Chem. Soc. Rev.*, 2015, **44**, 7128–7154.
 - 31 S. Tada, H. Nagase, N. Fujiwara and R. Kikuchi, What are the best active sites for CO₂ methanation over Ni/CeO₂?, *Energy Fuels*, 2021, **35**, 5241–5251.
 - 32 G. Zhou, H. Liu, K. Cui, A. Jia, G. Hu, Z. Jiao, Y. Liu and X. Zhang, Role of surface Ni and Ce species of Ni/CeO₂ catalyst in CO₂ methanation, *Appl. Surf. Sci.*, 2016, **383**, 248–252.
 - 33 L. Li, W. Zeng, M. Song, X. Wu, G. Li and C. Hu, Research progress and reaction mechanism of CO₂ methanation over Ni-Based catalysts at low temperature: A review, *Catalysts*, 2022, **12**, 244.
 - 34 H. Zhou, S. R. Docherty, N. Phongprueksathat, Z. Chen, A. V. Bukhtiyarov, I. P. Prosvirin, O. V. Safonova, A. Urakawa, C. Copéret, C. R. Müller and A. Fedorov, Combining atomic layer deposition with surface organometallic chemistry to enhance atomic-scale interactions and improve the activity and selectivity of Cu–Zn/SiO₂ catalysts for the hydrogenation of CO₂ to methanol, *JACS Au*, 2023, **3**, 2536–2549.
 - 35 M. Behrens, F. Studt, I. Kasatkin, S. Kühn, M. Hävecker, F. Abild-Pedersen, S. Zander, F. Girgsdies, P. Kurr, B.-L. Knief, M. Tovar, R. W. Fischer, J. K. Nørskov and R. Schlögl, The active site of methanol synthesis over Cu/ZnO/Al₂O₃ industrial catalysts, *Science*, 2012, **336**, 893–897.
 - 36 T. Lunkenbein, J. Schumann, M. Behrens, R. Schlögl and M. G. Willinger, Formation of a ZnO overlayer in industrial Cu/ZnO/Al₂O₃ catalysts induced by strong metal-support interactions, *Angew. Chem., Int. Ed.*, 2015, **54**, 4544–4548.
 - 37 S. Miyazaki, Z. Li, Z. Maeno, T. Toyao, M. Ito, Y. Nakajima and K. Shimizu, *Operando* Ce K-edge XANES study of low-loading Ni/CeO₂ in chemical looping dry reforming of methane, *Chem. Lett.*, 2022, **51**, 914–918.
 - 38 N. Rui, X. Zhang, F. Zhang, Z. Liu, X. Cao, Z. Xie, R. Zou, S. D. Senanayake, Y. Yang, J. A. Rodriguez and C.-J. Liu, Highly active Ni/CeO₂ catalyst for CO₂ methanation: Preparation and characterization, *Appl. Catal., B*, 2021, **282**, 119581.
 - 39 R.-P. Ye, Q. Li, W. Gong, T. Wang, J. J. Razink, L. Lin, Y.-Y. Qin, Z. Zhou, H. Adidharma, J. Tang, A. G. Russell, M. Fan and Y.-G. Yao, High-performance of nanostructured Ni/CeO₂ catalyst on CO₂ methanation, *Appl. Catal., B*, 2020, **268**, 118474.
 - 40 Y. Han, M. Tian, C. Wang, Y. Kang, L. Kang, Y. Su, C. Huang, T. Zong, J. Lin, B. Hou, X. Pan and X. Wang, Highly active and anticoke Ni/CeO₂ with ultralow Ni loading in chemical looping dry reforming via the strong metal-support interaction, *ACS Sustainable Chem. Eng.*, 2021, **9**, 17276–17288.
 - 41 J. Sun, S. Wan, F. Wang, J. Lin and Y. Wang, Selective synthesis of methanol and higher alcohols over Cs/Cu/ZnO/Al₂O₃ catalysts, *Ind. Eng. Chem. Res.*, 2015, **54**, 7841–7851.
 - 42 Y. Zhang, Q. Sun, J. Deng, D. Wu and S. Chen, A high activity Cu/ZnO/Al₂O₃ catalyst for methanol synthesis: Preparation and catalytic properties, *Appl. Catal., A*, 1997, **158**, 105–120.
 - 43 Q. Wang, Z. Yu, J. Feng, P. Fornasiero, Y. He and D. Li, Insight into the effect of dual active Cu⁰/Cu⁺ sites in a Cu/ZnO–Al₂O₃ catalyst on 5-hydroxymethylfurfural hydrodeoxygenation, *ACS Sustainable Chem. Eng.*, 2020, **8**, 15288–15298.
 - 44 H. Zhang, J. Chen, X. Han, Y. Pan, Z. Hao, S. Tang, X. Zi, Z. Zhang, P. Gao, M. Li, J. Lv and X. Ma, High-performance Cu/ZnO/Al₂O₃ catalysts for CO₂ hydrogenation to methanol, *Ind. Eng. Chem. Res.*, 2024, **63**, 6210–6221.
 - 45 S. B. Waghmode, R. Vetrivel, S. G. Hegde, C. S. Gopinath and S. Sivasanker, Physicochemical investigations of the basicity of the cation exchanged ETS-10 molecular sieves, *J. Phys. Chem. B*, 2003, **107**, 8517–8523.
 - 46 S. T. Yang, J. Kim and W. S. Ahn, CO₂ adsorption over ion-exchanged zeolite beta with alkali and alkaline earth metal ions, *Microporous Mesoporous Mater.*, 2010, **135**, 90–94.
 - 47 K. S. Walton, M. B. Abney and M. D. LeVan, CO₂ adsorption in Y and X zeolites modified by alkali metal cation exchange, *Microporous Mesoporous Mater.*, 2006, **91**, 78–84.
 - 48 R. Osuga, T. Yokoi and J. N. Kondo, Probing the basicity of lattice oxygen on H-form zeolites using CO₂, *J. Catal.*, 2019, **371**, 291–297.
 - 49 J. C. Lavalley, Infrared spectrometric studies of the surface basicity of metal oxides and zeolites using adsorbed probe molecules, *Catal. Today*, 1996, **27**, 377–401.
 - 50 G. Busca and V. Lorenzelli, Infrared spectroscopic identification of species arising from reactive adsorption of carbon oxides on metal oxide surfaces, *Mater. Chem.*, 1982, **7**, 89–126.
 - 51 R. W. Stevens, R. V. Siriwardane and J. Logan, *In situ* Fourier transform infrared (FTIR) investigation of CO₂ adsorption onto zeolite materials, *Energy Fuels*, 2008, **22**, 3070–3079.
 - 52 T. Riedel, M. Claeys, H. Schulz, G. Schaub, S.-S. Nam, K.-W. Jun, M.-J. Choi, G. Kishan and K.-W. Lee, Comparative study of Fischer–Tropsch synthesis with H₂/CO and H₂/CO₂ syngas using Fe- and Co-based catalysts, *Appl. Catal., A*, 1999, **186**, 201–213.
 - 53 X. Yin, D. Y. C. Leung, J. Chang, J. Wang, Y. Fu and C. Wu, Characteristics of the synthesis of methanol using biomass-derived syngas, *Energy Fuels*, 2005, **19**, 305–310.
 - 54 G. Liu, G. Yang, X. Peng, J. Wu and N. Tsubaki, Recent advances in the routes and catalysts for ethanol synthesis from syngas, *Chem. Soc. Rev.*, 2022, **51**, 5606–5659.
 - 55 B. B. Sahoo, N. Sahoo and U. K. Saha, Effect of H₂: CO ratio in syngas on the performance of a dual fuel diesel engine operation, *Appl. Therm. Eng.*, 2012, **49**, 139–146.
 - 56 A. Beck, M. A. Newton, L. G. A. van de Water and J. A. van Bokhoven, The enigma of methanol synthesis by Cu/ZnO/Al₂O₃-based catalysts, *Chem. Rev.*, 2024, **124**, 4543–4678.



- 57 G. Pacchioni, From CO₂ to methanol on Cu/ZnO/Al₂O₃ industrial catalyst. What do we know about the active phase and the reaction mechanism?, *ACS Catal.*, 2024, **14**, 2730–2745.
- 58 M. Behrens, F. Studt, I. Kasatkin, S. Kühl, M. Hävecker, F. Abild-Pedersen, S. Zander, F. Girgsdies, P. Kurr, B.-L. Knief, M. Tovar, R. W. Fischer, J. K. Nørskov and R. Schlögl, The active site of methanol synthesis over Cu/ZnO/Al₂O₃ industrial catalysts, *Science*, 2012, **336**, 893–897.
- 59 L. Guo, J. Sun, Q. Ge and N. Tsubaki, Recent advances in direct catalytic hydrogenation of carbon dioxide to valuable C₂₊ hydrocarbons, *J. Mater. Chem. A*, 2018, **6**, 23244–23262.
- 60 W. Zhou, K. Cheng, J. Kang, C. Zhou, V. Subramanian, Q. Zhang and Y. Wang, New horizon in C1 chemistry: breaking the selectivity limitation in transformation of syngas and hydrogenation of CO₂ into hydrocarbon chemicals and fuels, *Chem. Soc. Rev.*, 2019, **48**, 3193–3228.
- 61 S. Miyazaki, M. Yoshihara, T. Toyao, Z. Maeno and K. Shimizu, Continuous production of O₂-free enriched CO₂ from ambient air using moisture swing sorbents, *N. Nanotechnol.*, 2023, **3–4**, 100029.
- 62 S. Ullah, Y. Gao, L. Dou, Y. Liu, T. Shao, Y. Yang and A. B. Murphy, Recent trends in plasma-assisted CO₂ methanation: A critical review of recent studies, *Plasma Chem. Plasma Process.*, 2023, **43**, 1335–1383.
- 63 R. Döbek, F. Azzolina-Jury, A. Travert and F. Maugé, A review on plasma-catalytic methanation of carbon dioxide – Looking for an efficient catalyst, *Renewable Sustainable Energy Rev.*, 2019, **116**, 109427.

